Mueller Kim, Lynn (Orcid ID: 0000-0002-3516-2259)
Yadav Vineet (Orcid ID: 0000-0002-2805-3345)
Karion Anna (Orcid ID: 0000-0002-6304-3513)
Martin Cory (Orcid ID: 0000-0002-1546-9755)

Journal of Geophysical Research: Atmospheres

Siting background towers to characterize incoming air for urban greenhouse gas estimation: a case study in the Washington DC/Baltimore Area

K. Mueller[1,4], V. Yadav[3], I. Lopez-Coto[2], A. Karion[1], S. Gourdji[1,4], C. Martin[5,2], J. Whetstone[1]

[1] Special Programs Office, National Institute of Standards and Technology

[2] Fire Research Division, National Institute of Standards and Technology

[3] Jet Propulsion Laboratory

[4] Department of Climate and Space Science, University of Michigan

[5] Department of Atmospheric and Oceanic Science, University of Maryland

Corresponding author: Kim Mueller (kimberly.mueller@nist.gov)

Key Points:

- Factoring in the variability of greenhouse gas enhancements in incoming air is critical for estimating emissions in an urban domain.
- Statistical methods were used to site four towers sampling background air in the Washington DC/Baltimore region.
- Optimal background tower configurations for representing incoming air can still have large errors for any given urban GHG observation.

Abstract

There is increased interest in understanding urban greenhouse gas (GHG) emissions. To accurately estimate city emissions, the influence of extra-urban fluxes must first be removed from urban greenhouse gas (GHG) observations. This is especially true for regions, such as the U.S. Northeastern Corridor-Baltimore/Washington DC (NEC-B/W), downwind of large fluxes. To help site background towers for the NEC-B/W, we use a coupled Bayesian Information Criteria and geostatistical regression approach to help site four background locations that best explain CO_2 variability due to extra-urban fluxes modeled at twelve urban towers. The synthetic experiment uses an atmospheric transport and dispersion model coupled with two different flux inventories to create modeled observations and evaluate fifteen candidate towers located along the urban domain for February and July 2013. The analysis shows that the average ratios of extra-urban inflow to total modeled enhancements at urban towers are 21% to 36% in February and 31% to 43% in July. In July, the incoming air dominates the total variability of synthetic enhancements at the urban towers ($R^2 = 0.58$). Modeled observations from the selected background towers generally capture the variability in the synthetic CO_2 enhancements at urban towers ($R^2 = 0.75$, RMSE = 3.64 ppm; $R^2 = 0.43$, RMSE = 4.96 ppm for February and July). However, errors associated with representing background air can be up to 10 ppm for any given observation even with an optimal background tower configuration. More sophisticated methods may be necessary to represent background air to accurately estimate urban GHG emissions.

1 Introduction

Increased efforts to understand urban greenhouse gas (GHG) emissions have included the use of atmospheric GHG observations such as mole fractions measured at tower sites and by aircraft, satellite retrievals, and remotely sensed column-averaged dry mole fractions [Breón et al., 2015; Lauvaux et al., 2016; Boon et al., 2016; Cambaliza et al., 2014, etc.]. Coupling such observations with atmospheric transport and dispersion models and prior understanding of urban emissions to estimate surface fluxes, is referred to as a top-down analysis, as opposed to a bottom-up approach that relies on emission inventories or process-based modeling. To use top-down methods effectively to estimate urban emissions, the influence of atmospheric carbon dioxide (CO_2) or methane (CH_4) originating from sources and sinks outside the metropolitan area must first be isolated and subtracted from mole fractions observed in the city [Turnbull et al., 2015].

Previous urban top-down inverse modeling studies have used relatively simple approaches, e.g. mole-fractions measured at upwind tower locations [e.g. Lauvaux et al., 2016; Breón et al., 2015; McKain et al., 2015] or sites that sample clean air [e.g. Verhulst et al., 2016], to represent incoming air. In practice, the use of observations from background sites or towers to represent the inflow of background GHG air has had limited success for estimating urban emissions in a top-down framework. For example, estimates of city emissions in the dormant season, that are not complicated by an active biosphere outside the metropolitan area, have been

shown to be sensitive to the choice of the background mole fraction even in urban domains that are more isolated from other cities [e.g. Lauvaux et al., 2016; Turnbull et al., 2015]. As such, simple approaches may not properly represent background air if they can't account for the variability associated with (1) complex meteorology upwind and across a city and (2) spatially and temporally changing extra-urban fluxes.

At present, there aren't simple methods for translating these background errors, or any other errors, into their impact on estimated emissions without conducting inversion experiments. Future work will need to elucidate how these errors manifest themselves both in spatially and temporally explicit emission estimates as well as in total city emission averages. Nevertheless, we know that properly representing the inflow of GHGs to urban areas is a crucial element in estimating urban GHG emissions [Turnbull et al., 2015], yet a standard approach to select background tower locations and assess their performance does not exist for top-down inversion methods.

The purpose of this study is to identify the location of up to four tower-based observing points that best explain CO_2 mole fractions of incoming air to the Washington, D.C. and Baltimore, Maryland urban area, referred to as the Northeastern Corridor-Baltimore/Washington DC (NEC-B/W). Unlike the simple approaches mentioned earlier, this method accounts for variability in both the fluxes outside of the urban domain as well as regional meteorology. We consider establishing a maximum of four towers given logistical and cost constraints. The background tower selection method presented here could account for similar constraints in other urban studies. For locations like the NEC-B/W, estimating the incoming GHG mole fractions is more important than for other areas because the region is downwind of major regional sources (e.g., power plants and other industrial emitters that are in the adjacent states of Pennsylvania, Virginia, and West Virginia) as well as significant biogenic fluxes (Figure 1) and is entangled within other urban areas along the Northeastern coast. Thus, the background tower selection method is a critical component for estimating urban GHG emissions using an inversion framework for metropolitan areas like the NEC-B/W.

This work focuses on better understanding and characterizing CO_2 entering the NEC-B/W domain due to the spatial and temporal variability of the meteorology and fluxes outside of the urban area. We are particularly focused on how this variability manifests itself in mole fraction measurements from urban towers in the NEC-B/W. We employed a simulation analysis of candidate background observational sites located on communications towers outside the NEC-B/W along with urban tower locations identified by Lopez-Coto et al. [2017]. The method presented in this paper is not specific to CO_2 and thus can be applied to other trace gases as well, if meteorological information and realistic prior flux information is available.

1.1 Description of the Northeastern Corridor – Baltimore, Washington DC

The NEC-B/W domain considered in this work comprises the urban and suburban areas of Washington, DC and Baltimore, Maryland (Figure 1). This area is the most recently-established

of three National Institute of Standards and Technology (NIST) urban GHG measurements testbeds (the others being INFLUX in Indianapolis and the Megacities project in Los Angeles) [Davis et al., 2017; Duren et al., 2012]. As with the other testbed sites, current NEC-B/W efforts are focused on establishing a tower-based, in-situ GHG mole fraction observing network of 16 towers (12 urban sites in the urban domain in the blue box in Figure 1 as informed by Lopez-Coto et al., [2017] and 4 background sites near the perimeter of the domain whose locations are being investigated in this work) to measure CO_2 and CH_4 due to emissions in the metropolitan area.

Top-down approaches will be a significant component of the proposed effort, including the development of an inversion framework for CO_2 and CH_4 flux estimation. The desired CO_2 flux estimation resolution is like that of the other two testbeds [e.g. Lauvaux et al., 2016], i.e. monthly or sub-monthly, 1-2 km^2 estimates that have accuracy levels of at least 10%. Given that the NEC-B/W is located on the eastern edge of the continental United States, it is anticipated that the in-domain CO_2 mole fraction measurements will be strongly influenced by upwind regional sources and sinks. Thus, emission estimates from an atmospheric inversion framework can be significantly biased if the influence of extra-urban fluxes transported to the in-domain observing locations is not isolated from observations.

1.2 Potential Background Tower Locations

As noted earlier, this work applies a statistical approach to inform the choice of locations that help explain the background portion of the mole fractions measured at towers in the NEC-B/W. Before these methods can be applied, potential locations for background towers need to be identified among existing communications towers, all of which are contained in the Federal Communications Commission (FCC) database (http://wireless2.fcc.gov/). The database was filtered based on tower height (~100m or greater) and distance (> 10 km) to major roads or large point sources such as power plants. The filter resulted in 15 candidate locations in areas around the NEC-B/W urban domain as shown in Figure 1.

2 Methods

A mole fraction observed at a NEC-B/W urban tower location is composed of individual components as per Equation 1:

$$\boldsymbol{y} = \boldsymbol{y}_{continental} + \boldsymbol{y}_{fossil\_ex} + \boldsymbol{y}_{bio\_ex} + \boldsymbol{y}_{fossil\_urb} + \boldsymbol{y}_{bio\_urb} \quad (1)$$

Where $\boldsymbol{y}$ is a time series vector of GHG mole fractions, in units of μmol CO_2 $per\ mol$ dry air or parts per million (ppm), associated with the NEC-B/W tower locations in the urban domain (Figure 2, blue boundary) and $\boldsymbol{y}_{continental}$ represents the well-mixed and homogeneous incoming global and continental GHG air mass entering the outer domain (Figure 2, thick black boundary). This $\boldsymbol{y}_{continental}$ component is assumed to be relatively uniform across the NEC-B/W having

minimal impact on GHG urban emissions estimates as it should be easily removed from $\boldsymbol{y}$ using in-situ or flask measurements from established sites across the U.S.

The CO_2 mole fraction associated with anthropogenic sources in the NEC-B/W domain, $\boldsymbol{y}_{fossil\_urb}$, is the portion of the observational signal needed to accurately estimate GHG emissions in the NEC-B/W domain. The contribution to $\boldsymbol{y}$ due to biospheric fluxes inside the domain, $\boldsymbol{y}_{bio\_urb}$, is also an important contributor. In future work, $\boldsymbol{y}_{bio\_urb}$ will need to be appropriately identified and removed from $\boldsymbol{y}$ to isolate $\boldsymbol{y}_{fossil\_urb}$ so that anthropogenic emission estimates are not biased, but it is not considered in this analysis. Most important to this work are $\boldsymbol{y}_{fossil\_ex}$ and $\boldsymbol{y}_{bio\_ex}$, which are mole fractions associated with the NEC-B/W towers attributable to sources and sinks located up to 550 km outside the NEC-B/W boundary (Figure 2). Unlike $\boldsymbol{y}_{continental}$, these contributions are not considered to be spatially or temporally homogeneous or well-mixed. The 550 km domain was chosen to be consistent with the Lopez-Coto et al. [2017] urban tower selection study.

We express the background mole fraction (i.e. the mole fraction enhancement due to sources between the extra-urban and urban domains), as observed at a given NEC-B/W tower as:

$$\boldsymbol{y}_{ex} = \boldsymbol{y}_{fossil\_ex} + \boldsymbol{y}_{bio\_ex} \quad (2)$$

The purpose of this work is to identify a set of background tower locations so that the combination of their mole fractions equates to $\boldsymbol{y}_{ex}$. Henceforward, subscripts (i) and (j) will be used respectively to refer to a specific urban (where i = 1 ... 12) or background tower (where j = 1 ... 15).

2.1 Synthetic Data

Synthetic data are used in this study to select tower locations whose modeled observations will best represent the CO_2 coming into the NEC-B/W region as discussed above. Synthetic data allow us to examine how the variability of extra-urban fluxes and meteorology will likely manifest itself in the NEC-B/W urban observations without the influence of other error sources. The simulated data correspond to an accepted and realistic model for atmospheric transport and dispersion and are the basis for selecting the background towers that will be used to represent $\boldsymbol{y}_{ex}$. The synthetic enhancements of CO_2 for each of the 12 NEC-B/W tower locations are the product of the strength and number of sources and sinks between the extra-urban (black, Figure 2) and urban (blue, Figure 2) domains, meteorology (e.g. wind direction and speed) and dispersion. Synthetic data are created for February and July 2013, representing typical winter and summer time periods where meteorological conditions and regional fluxes significantly differ from each other. The Supplementary Information contains a detailed explanation as to how the synthetic observations are generated; the following paragraphs provide a brief description.

To create the synthetic observations ($\boldsymbol{y}_{ex}$ and $\boldsymbol{y}_{urb}$), Weather Research & Forecast (WRF) modeled output (details in Lopez-Coto et al., [2017]) is used in conjunction with the Stochastic Time Inverted Lagrangian Transport (STILT) model [Lin et al., 2003], which is based on NOAA's HYSPLIT algorithm [Stein et al., 2015]. These transport and dispersion models are used to estimate sensitivities of hourly observations to surface fluxes (units of $\frac{ppm}{\mu mol/m^2 s}$), referred to as footprints or the matrix $\boldsymbol{H}_{i=1..12}$, where i designates one of the twelve NEC-B/W towers. To create synthetic observations, the footprints are convolved with fossil fuel CO_2 emissions from Vulcan v2.2 ($\boldsymbol{s}_{fossil\_ex}$ in Equation 3 and $\boldsymbol{s}_{fossil\_urb}$ in Equation 4) provided at http://vulcan.project.asu.edu/ [Gurney at al., 2009]. Biospheric fluxes are from NOAA's Earth System Research Laboratory's CarbonTracker (CT) 2013b model (denoted as $\boldsymbol{s}_{bio\_ex}$ in Equation 3 and $\boldsymbol{s}_{bio\_ex}$ in Equation 4) sourced at http://carbontracker.noaa.gov [Peters et al., 2007]. The model resolutions for Vulcan v2.2 and CarbonTracker 2013b are described in the Supplemental Information and their monthly averaged fluxes are shown in Figure 5c and 5d.

The convolutions (Equations 3 and 4) result in synthetic observations that represent the background CO_2 mole fractions at the twelve NEC-B/W tower locations (henceforward referred to as $\boldsymbol{y}_{ex\_i}$). In Equation 3, only fluxes between the outer (black, Figure 2) and the inner (blue, Figure 2) domains are used in the convolution.

$$\boldsymbol{y}_{ex\_i} = \boldsymbol{H}_i \boldsymbol{s}_{fossil\_ex} + \boldsymbol{H}_i \boldsymbol{s}_{bio\_ex} \quad (3)$$

In a similar manner to Equation 3 for $\boldsymbol{y}_{ex\_i}$, synthetic observations are created at each NEC-B/W location using fluxes inside the urban domain ($\boldsymbol{s}_{fossil\_urb}$ and $\boldsymbol{s}_{bio\_urb}$) in the blue pixels in Figure 2, referred to as $\boldsymbol{y}_{urb\_i}$.

$$\boldsymbol{y}_{urb\_i} = \boldsymbol{H}_i \boldsymbol{s}_{fossil\_urb} + \boldsymbol{H}_i \boldsymbol{s}_{bio\_ex} \quad (4)$$

$\boldsymbol{y}_{ex\_i}$ and $\boldsymbol{y}_{urb_i}$were generated for afternoon hours only (i.e. noon to 5pm local standard time). Most urban and regional inversion studies (e.g. Lauvaux et al., 2016 and Gourdji et al., 2012) use afternoon observations given that a changing planetary boundary layer or night time conditions are difficult to model and thus, would yield errors that would significantly bias emission estimates.

Synthetic observations (referred to henceforward as $\boldsymbol{z}_j$) are also generated for all hours of the day, not just mid-afternoon hours, at candidate background towers using footprints ($\boldsymbol{H}_{j=1..15}$) and fluxes ($\boldsymbol{s}_{fossil\_ex}$ and $\boldsymbol{s}_{bio\_ex}$).

2.1.1 Creating Background Time Series Corresponding to NEC-B/W Tower Observations

Given that it takes time for a STILT modeled particle to traverse the NEC-B/W domain (approximately four to six hours), we want to ensure that the background site will first "see" and observe time-varying background concentrations before reaching the urban site several hours later. Thus, a background tower's observations ($\boldsymbol{z}_j$) must be adjusted to properly synchronize it

with a NEC-B/W tower's background observations ($\boldsymbol{y}_{ex\_i}$). For every NEC-B/W tower receptor, an average time (Δt) is estimated to account for transit time of 1000 STILT particles to traverse from the NEC-B/W boundary to a NEC-B/W tower location based on the wind speed, direction and vertical mixing from WRF-STILT. The average location where particles entered the NEC-B/W domain is also noted to identify the closest background tower sites for each receptor. Each selected background tower time series ($\boldsymbol{z}_j$) is shifted in accordance by ($\Delta t_{i,j}$), henceforward referred to as $\boldsymbol{z}_{j\_i}$. In $\boldsymbol{z}_{j\_i}$, a selected background tower (j) is associated with a specific NEC-B/W tower (i) observational time series.

2.2 Selection Approach

This approach to background tower site selection uses geostatistical regression coupled with a model selection algorithm (methods employed in Mueller et al., [2010] and Yadav et al., [2010]). Note, since $\boldsymbol{y}_{ex}$ consists of only afternoon hour observations associated with well mixed conditions, we cannot employ more conventional time series approaches that require equally spaced measurements without gaps. The geostatistical regression, analogous to linear regression, expresses the dependent variable, in this case the synthetic background CO_2 mole fractions associated with NEC-B/W tower locations or $\boldsymbol{y}_{ex}$, as the sum of a deterministic component and a stochastic term. In the regression, the deterministic component represents the part of the CO_2 modeled observations that can be explained using a set of covariates (in this case, combinations of observations from the background towers). In the setup, the stochastic component, which is the portion of $\boldsymbol{y}_{ex}$ that is not explained by the deterministic component (i.e. the modeled observational residuals), is assumed to be temporally correlated with an expected value of zero, a reasonable assumption for CO_2 time-series observations. As per previous works using CO_2 mole fraction time series [e.g. Lauvaux et al., 2016; Yadav et al., 2010; Gourdji et al., 2012; Mueller et al., 2010], an exponential covariance function is used to model the stochastic component.

The deterministic component takes the form of a model of the trend (i.e. $\mathbf{X\beta}$). For the geostatistical regression, the $\mathbf{X}$ matrix contains up to four covariates or columns, i.e. vectors of background tower synthetic observations for a NEC-B/W tower (i) of interest, i.e. $\boldsymbol{z}_{j\_i}$. These vectors are scaled by unknown drift coefficients ($\boldsymbol{\beta}$). The geostatistical regression is used to obtain the best estimate of the unknown drift coefficients, $\widehat{\boldsymbol{\beta}}$, and their corresponding variance, $\sigma^2_{\widehat{\boldsymbol{\beta}}}$. These represent the relationship between the observational time series for a NEC-B/W tower ($\boldsymbol{y}_{ex}$) and each vector (i.e. $\boldsymbol{z}_{j\_i}$ candidate background tower timeseries) as described in further detail in the following subsection.

2.2.1 Bayesian Information Criterion (BIC)

The geostatistical regression algorithm (as explained in Section 2.2.2) is applied after the synthetic mole fractions from every four-column combination of the fifteen candidate

background towers are investigated using the Bayesian Information Criterion (BIC) model selection algorithm. The first step of applying the BIC method is to create a matrix for each of the twelve NEC-B/W towers (i.e. $\mathbf{X}_i$) for February and July that contains mole fractions from each of the fifteen candidate background towers. An example of $\mathbf{X}_i$, an (m x 15) matrix where m is the number of observations in $\boldsymbol{y}_{ex}$, is provided below:

$$\boldsymbol{X}_{\mathbf{VA1}} = [\boldsymbol{z}_{\mathbf{BG1\_VA1}} \quad \cdots \quad \boldsymbol{z}_{\mathbf{BG15\_VA1}}], \tag{5}$$

where $\boldsymbol{z}_{\mathbf{BG1\_VA1}}$ refers to a vector of modeled CO_2 mole fractions observed at background tower BG_1 associated with those from NEC-B/W tower VA_1. Once twelve $\mathbf{X}_i$ are constructed (one for each NEC-B/W tower location), two ($12 * m$ x 15) $\mathbf{X}_{full}$ matrices and one ($12 * m$ x 1) $\boldsymbol{y}_{ex}$ vector are assembled by vertically concatenating all twelve $\mathbf{X}_i$ matrices and $\boldsymbol{y}_{ex\_i}$ vectors for February and July.

To identify the ideal background tower locations, the fifteen columns of $\mathbf{X}_{full}$ are used to construct combinations of $\mathbf{X}$ matrices. Since we are searching for up to four sites, each $\mathbf{X}$ contains up to four columns. Instead of considering all fifteen background towers for any given hourly receptor, we only allow the algorithm to choose from those towers that are closest, approximately 100 km away, to where the particles on average leave the urban domain (blue box in Figure 2, explained in Section 2.1.1) for a certain observational time. By examining different combinations of mole fractions as observed at background towers, instead of using a single regressor (i.e. mole fractions from a single background tower), we can assess the best configuration of background towers whose mole fractions best explain the variability in $\boldsymbol{y}_{ex}$.

In this study, as in Mueller et al., [2010] and Yadav et al., [2010], the BIC provides a metric for selecting the best sets from modeled $\boldsymbol{z}_{j\_i}$ of up to four background towers by ranking how well each $\mathbf{X}$ explains the variability in $\boldsymbol{y}_{ex}$. However, we can't rely on the BIC and models alone to determine the final set of background towers since most of the columns of $\boldsymbol{z}_{j\_i}$ in $\mathbf{X}_{full}$ are highly correlated. This results in likelihoods that are not significantly different between models. Nonetheless, the BIC metric helps us narrow the number of candidate models so that we do not need to examine every regression subset of $\boldsymbol{z}_{j\_i}$. To complement the BIC analysis, we employ a geostatistical algorithm to help site background towers as explained in the following section. More information, including equations for the BIC and Geostatistical Regression, are provided in the Supplementary Information.

2.2.2 Geostatistical Regression

The estimated drift coefficients (henceforward referred to as scaling factors), $\widehat{\boldsymbol{\beta}}$, for each column of $\boldsymbol{z}_{j\_i}$ in $\mathbf{X}$ and their associated uncertainty covariance ($\mathbf{V}_{\widehat{\boldsymbol{\beta}}}$) are also used, along with the BIC metric, to help select the four suitable background tower locations. $\boldsymbol{V}_{\widehat{\boldsymbol{\beta}}}$ is a matrix which provides the variances associated with a scaling factor for a single $\boldsymbol{z}_{j\_i}$ column along with the covariance between scaling factors. Given the high degree of co-linearity in $\mathbf{X}$, the covariance

between the scaling factors provides a measure of independence between the selected background tower observations in terms of their ability to explain the variability in $\boldsymbol{y}_{ex}$. This allows us to locate background towers whose mole fractions maximally improve background CO_2 at the NEC-B/W tower observations. In addition, the scaling factors, $\widehat{\boldsymbol{\beta}}$, along with their associated uncertainties, i.e. $\boldsymbol{\sigma}_{\widehat{\boldsymbol{\beta}}}$, help indicate which background towers tend to significantly explain most of the variability associated with the incoming air.

3 Data Analysis: Variability of Incoming Air

Before candidate background towers can be selected, it is important to understand (1) how modeled CO_2 mole fractions in the incoming air compare to atmospheric CO_2 enhancements associated with sources and sinks inside the NEC-B/W domain as well as (2) the characteristics of the background CO_2 mole fraction entering the NEC-B/W domain. Some specific questions regarding background air characteristics include: from where is the inflow primarily originating, and can sub-groups of NEC-B/W towers observations explain similar types of incoming CO_2? Answering both questions will help justify the siting of background tower locations.

3.1 Comparison of Background Mole Fractions and CO_2 Enhancements Due to Emissions Inside the NEC-B/W

The enhancements at the tower sites due to incoming CO_2 from the extra-urban domain have a measurable but seasonally dependent impact on both the overall CO_2 magnitude and variability at the NEC-B/W towers (Figure 3). The average mole-fraction ratio across towers of atmospheric CO_2 inflow ($\boldsymbol{y}_{ex}$) to the total modeled enhancement (aka $\boldsymbol{y}_{tot} = \boldsymbol{y}_{urb} + \boldsymbol{y}_{ex}$) are 29% and 43% for February and July respectively, with ranges of 21% to 36% in winter and 31% to 56% in summer. It is noticeable that there is less variability in $\boldsymbol{y}_{ex}$ relative to $\boldsymbol{y}_{tot}$ in February ($R^2 = 0.05$) compared to July ($R^2 = 0.58$) (Figure 3). R^2 values between $\boldsymbol{y}_{tot}$ and $\boldsymbol{y}_{ex}$ vary across the different urban towers in both months with largest correlations in July (R^2 range from 0.55 (BA_3) to 0.87 (VA_3)). Although it is important to account for incoming air in both winter and summer months, these results demonstrate that properly representing incoming air will be more important in the summer for areas like the NEC-B/W.

The variability in July, and the negative values associated with $\boldsymbol{y}_{ex}$, are likely a result of an active biosphere and variable meteorology (Figure 4). Beyond being clustered with other eastern U.S. metropolitan areas, the NEC-B/W is surrounded by deciduous forests especially on its western, Northwestern, and Southwestern boundaries. It is also downwind of intensive agricultural areas such as Ohio where corn, soy beans, and alfalfa are grown. These biogenic sources and sinks constitute up to 20% (February) and 35% (July) of the average CO_2 in the simulated background air at NEC-B/W towers. Of course, this varies by the location and height of the tower.

3.2 Origins of Incoming Air Mass as Observed at NEC-B/W Tower Locations

Although the ratio of $\boldsymbol{y}_{ex\_i}$ to $\boldsymbol{y}_{tot\_i}$ varies by tower, NEC-B/W towers may observe similar modeled background CO_2 mole fractions depending on the meteorology and temporally varying extra-urban fluxes. We investigate similarities and differences in the NEC-B/W tower background observations $\boldsymbol{y}_{ex\_i}$ using correlation coefficients (ρ) and root mean squared difference (RMSD) metrics to help group NEC-B/W towers. In this manner, we correlate and compare each of the twelve NEC-B/W mole fractions with simulated observations from the other eleven tower locations. Identifying groups provides a measure of the number of background tower locations necessary to explain the incoming CO_2 mole fractions for the NEC-B/W tower observations as a whole.

The analysis yielded three expected groups of towers (Figure 4): (1) those clustered in the Baltimore region (red squares, ρ = 0.92 and RMSD = 1.67 in February, ρ = 0.83 and RMSD = 2.22 in July), (2) those concentrated around Washington DC and northern Virginia (orange circles, ρ = 0.89 and RMSD = 1.47 in February, ρ = 0.83 and RMSD = 1.95 in July), and (3) those located between Baltimore and Washington DC that didn't fall into any of the previously identified groups (gray triangles). Lower correlations and higher RMSD values between groups one and two (ρ = 0.60 and RMSD = 3.19 ppm in February, ρ = 0.43 and RMSD = 3.84 ppm in July), further suggest that these two clusters of towers observe differences in the origins of background air.

The grouping of different towers based on the variations in the simulated NEC-B/W CO_2 enhancements demonstrates that each $\boldsymbol{y}_{ex\_i}$ can have different sensitivity to the underlying extra-urban flux variability. This result is consistent with other studies that found that atmospheric CO_2 observations from individual continental in-situ observational sites can be sensitive to the fine scale spatial and temporal variability of 1 degree biogenic fluxes in large ecoregions in the far field [Gourdji et al., 2012; Huntzinger et al., 2011; Fang et al., 2014]. Hence, it is expected that the number and configuration of background towers will be dependent on how much extra-urban flux variations, both in space and time, manifest themselves in the NEC-B/W observed mole fractions at the different urban tower locations. The NEC-B/W tower groupings result shows that, even if the mole fractions from a configuration of background towers capture background air on average, the fine scale spatial and temporal extra-urban flux variability may still prove problematic for estimating urban emissions.

To further investigate the impact of regional flux variability on $\boldsymbol{y}_{ex}$, we assess the spatial and temporal variations in the modeled background contributions (in ppm) from each flux location on the NEC-B/W observations ($\boldsymbol{y}_{ex\_i}$). These contributions result from the dot product of footprints (units of $\frac{ppm}{\mu mol/m^2 s}$) and regional fluxes ($\boldsymbol{s}_{fossil\_ex} + \boldsymbol{s}_{bio\_ex}$, units of $\mu mol/m^2 s$), which is simply the multiplication of every flux by its corresponding sensitivity in $\boldsymbol{H}_i$. Depending on the wind regime and the height of the planetary boundary layer (PBL), a given NEC-B/W tower-observed CO_2 enhancement is sensitive to different regional fluxes over time

and, thus, the spatial extent and shape of the background contributions are expected to change through the month.

As expected, the two primary groups of NEC-B/W tower locations tend to observe background CO_2 enhancements from sources and sinks in their respective upwind areas of prevailing winds during February and July. For example, BA_4 in Group 1 tends to observe, on average, more background air from sources and sinks from the north and northwest, such as those in eastern Pennsylvania (Figure 5b), compared to VA_1 in Group 2 (Figure 5a), which is influenced more by fluxes in Virginia and North Carolina for February. Thus, each $\boldsymbol{y}_{ex\_i}$ "sees" different parts of the underlying spatial distribution of extra-urban fluxes. For example, parts of Pennsylvania have a dissimilar influence on the modeled CO_2 enhancements from one NEC-B/W location compared to those associated with another tower site.

To further investigate the relative spatial and temporal influence of fluxes on observed mole fractions as a function of distance, we adopt common terms used in the inversion literature, i.e. the near field and far field. Gerbig et al. [2009] define the near field as the area within about 50 km from a measurement location. It is well known that the spatial variations of near field surface fluxes contribute significantly to the variability in observed CO_2 [e.g. Gerbig et al., 2003b, 2009; Huntzinger et al., 2011]. We include an additional classification, i.e. the intermediate field which are fluxes that are 300 km from the edge of the NEC-B/W domain while defining the far field as sources and sinks 300 km (thick dashed magenta rectangle in Figure 2) to 550 km away (550 km is the edge of the thick black rectangle in Figure 2). We assume that all near field fluxes are in the urban domain given that the width the NEC-B/W is approximately 120 km and, thus, not considered. Monthly background contributions to all NEC-B/W tower background observations are binned by their originating sector: north, northeast, east, southeast, south, southwest, west, northwest. The analysis explores the temporal impact of extra-urban fluxes on the variability of NEC-B/W mole fractions as a function of their distance away from NEC-B/W tower locations.

Predictably, the contribution of background air to the NEC-B/W observations is dependent upon the time of the year. However, even though the sources and sinks from 300 km (intermediate field) to 550 km (far field) from the urban domain may, on average, have a small contribution to the modeled enhancements, there are instances when they have a large impact. The boxplots in Figure 6 show most of the incoming CO_2 originates from the Northwest and West in February with substantial outliers resulting from fluxes and inflow from the North and Northeast. As mentioned earlier, this behavior corresponds to weather patterns typical of winter in the mid-latitudes, where the dominant flow is westerly but may shift to northerly and northeasterly as storms exit. However, in July, CO_2 enters the NEC-B/W from multiple locations, with no single predominant direction (Figure 6). The far field in both months can be as important, if not more important, in terms of its impact on the variability in the NEC-B/W observed mole-fractions. For example, Figure 6 shows several extreme outlier contributions to the NEC-B/W CO_2 enhancements from the North and Northwest in February and from the

Northeast, North, and South for July even though the median contribution is negligible. The high sensitivity of the signals to slight differences in time varying fluxes in the intermediate and far field demonstrates the importance of accurately representing small-scale temporal variability using observations from background towers.

The work presented thus far, although informative regarding the nature and origin of CO_2 in incoming air, suggests that a more rigorous method is needed to site background tower locations for the NEC-B/W project given the spatial and temporal variability in $\boldsymbol{y}_{ex}$. However, the analysis does demonstrate that at least two or three background towers are needed to explain the variability in incoming CO_2 concentrations observed by the groups of NEC-B/W towers shown in Figure 4.

4 Results

To complement the data analysis, the following section presents the results from using the BIC and geostatistical regression method to identify background tower locations that best explain the variability in the background air as observed at the NEC-B/W towers.

4.1 Background Towers Selected by BIC Method and Geostatistical Regression

Results from the BIC algorithm indicate that four background towers are significantly better than two (57% more likely) and marginally better than three (29% more likely) at capturing the variability in incoming CO_2 as observed by the NEC-B/W towers. Given that different combinations of mole fractions from four towers are not significantly different from one another at the 95% confidence level, additional analysis of the background tower scaling factors, $\widehat{\boldsymbol{\beta}}$, and their associated variances, $\boldsymbol{V}_{\widehat{\boldsymbol{\beta}}}$, is warranted to help inform the choice of background tower locations. The geostatistical regression analysis allows us to investigate how much the mole fractions from a given background tower explain the variability in $\boldsymbol{y}_{ex}$ within a specific model. The resultant top models from BIC analysis represent the combinations of four towers that best explain the observed mole fraction variability in $\boldsymbol{y}_{ex}$. The approach involves separate analyses that use background towers associated with NEC-B/W Group 1, Group 2 (as shown in Figure 4), and all twelve towers for February and July.

As expected, the selected and significant background tower observations (as identified by a * or ** in Table 1) are different for the winter and summer months as determined through the coupled BIC and geostatistical regression. From the top models as selected by the BIC method, the observations associated with background towers along the Western and Northwestern edges of the domain appear to be significant in capturing incoming CO_2 to the NEC-B/W urban area in February. However, the results for July are much less conclusive, especially for results associated with the groups of towers. For the combined results, where there is more statistical power, mole fractions simulated for towers on Northern, Southwestern, and Southern boundaries explain $\boldsymbol{y}_{ex}$, a result that reflects the variability noted earlier of $\boldsymbol{y}_{ex}$ during this summer month.

Overall, simulated observations at background towers BG_1, BG_2, and BG_8 best capture the variability in $\boldsymbol{y}_{ex}$. The top model combinations, as identified by BIC algorithm, consistently contain these background sites and their associated scaling factors are significant at the 66% and 95% confidence levels (Table 1). The covariances between the scaling factors associated with simulated observations from three background towers (as estimated in $\boldsymbol{V}_{\widehat{\boldsymbol{\beta}}}$) indicate that these towers have relatively independent representations of background CO_2 inflow. Other towers also are significant but they are not as persistent across models as background towers 1, 2, and 8 across all three categories. Based on this analysis, these locations are chosen as optimal sites to install background towers.

Two other candidate towers along the Southern urban edge, i.e. BG_5 and BG_7, are also considered possibilities as they are consistently selected in the top model combinations for the Combined category in Table 1. To help discern between siting a background tower at BG_5 or BG_7, R^2 values are estimated for two model combinations. Both models contain modeled time-series from background towers 1, 2, and 8 but one contains simulated mole fractions from background tower 5 and the other mole fractions from background tower 7. Background tower 5, due South of the domain, has a larger R^2 value, especially in July (from 0.2 to 0.52), and thus is considered the preferable location for the fourth background tower.

4.2 The Ability of Background Tower Measurements to Explain Background Air Mole Fractions

R^2 and RMSE metrics are used to assess the ability of the observed mole fractions at background towers 1, 2, 5 and 8 to explain the variability of the background mole fractions at the NEC-B/W tower locations ($\boldsymbol{y}_{ex}$). For this analysis, an upwind background value time series is generated using the observations from the closest of the four background towers from where the averaged particles (generated in Section 2.1 and 2.2) enter the urban domain. This constructed mole fraction time series is henceforward referred to as the modeled background. $\boldsymbol{y}_{ex}$ is used as the "truth" for comparison. Ideally, if the four background towers perfectly explained $\boldsymbol{y}_{ex}$, we would expect the R^2 values to be one and the RMSE to be zero. We do not use the linear combination for our modeled background, i.e. $\mathbf{X}\widehat{\boldsymbol{\beta}}$, since $\widehat{\boldsymbol{\beta}}$ would not be known in a real data inversion application.

The R^2 and RMSE indicate that the ability of the four chosen background tower sites (i.e. modeled background) to explain incoming CO_2 as observed at NEC-B/W towers (aka the "truth" in this synthetic data experiment) is seasonally and spatially dependent. The winter month has a larger R^2 (0.75) than the summer month (R^2 = 0.53) because the biogenic fluxes outside of the NEC do not significantly contribute to mole fractions observed at the NEC-B/W tower locations in February. The RMSE is lower for February (3.64 ppm) compared to July (4.96 ppm) and the average ratio of the modeled background to the total observed mole fraction is 34% at the NEC towers in both February and July. When the four background towers are used to explain the incoming CO_2 observed at NEC-B/W towers, there is a small negative bias (-0.84 ppm) in

February and a positive bias in July (1.10 ppm). These biases would result in larger and smaller than expected estimated CO_2 emissions for respective winter and summer months.

The modelled background overall explains the true background, but for any given observational time, the modeled background can deviate substantially from the truth (i.e. $\boldsymbol{y}_{ex}$), sometimes by as much as 10 ppm (Figure 7). Since the RMSE and correlation coefficients provide average metrics, they can disguise large errors that can significantly impact urban GHG estimations in an area such as the NEC-B/W, especially if the errors are not random and are correlated in time as suggested by Figure 7. Thus, to avoid large temporal aggregation errors (and biases), inversions that use background tower mole fractions to represent incoming air, should account for the fine scale variability in the observations in some way. This may include resolving emissions at fine temporal scales.

5 Discussion

The BIC algorithm and geostatistical method presented are meant to demonstrate a statistical approach to inform the selection of background tower locations for an urban GHG estimation inversion analysis. However, logistical constraints are also important in deciding where to establish background tower locations. In the case of the NEC-B/W region, it was determined that an already established tower in Bucktown, Maryland operated by Earth Networks (www.earthnetworks.com) since 2011 (aka GHG01 located at the southeastern edge outside of the NEC-B/W domain for which NIST has data access – see Figure 1) informs some of the southern CO_2 airflow as seen by BG_5 based on footprint analysis (not shown). Thus, it was determined that BG_7 would be used with BG_1, BG_2, and BG_8 instead of BG_5. In this manner, GHG01 operates as a fifth background tower site for the NEC-B/W.

Nevertheless, even if background towers are ideally located, challenges exist in capturing atmospheric CO_2 inflow mole fraction into an urban region such as the NEC-B/W using towers alone. Indeed, multiple background tower locations better characterize incoming CO_2 mole fractions than a single location. However, the vertical and horizontal heterogeneous structure of the mole fractions along metropolitan boundaries (70 km – 150 km in length) due to changing meteorology and extra-urban sources and sinks challenge representation of incoming CO_2 using a handful of fixed locations. In temperate regions, such as this one, strong biogenic activity during the growing season creates large diurnal and seasonal variability in the incoming CO_2 mole fractions that is particularly challenging to capture with a limited and fixed set of background tower observations as discussed in Section 3.1. This result is reflected in the degraded performance of the modeled background in July relative to February (higher RMSE and lower correlation coefficients in Figure 7).

Additionally, urban inversion studies face unique difficulties in using background towers in a Lagrangian framework to represent incoming GHG mole fractions. Observations from towers outside the urban region are impacted by local atmospheric dynamics impairing their spatial and temporal representation of background air. In addition, observed mixing ratios

upwind at earlier time periods can be impacted by local meteorological conditions, such as a shallow boundary layer or complex meteorology. The inability of the Lagrangian framework to model these dynamics may lead to larger errors. To investigate this further, we forecast CO_2 concentrations in four-dimensions (10 min, 1km horizontally with 50 vertical levels, 30 of which are clustered in the lowest 20% of the atmosphere) at the boundaries of the NEC-B/W domain (blue box in Figure 1) using WRF-Chem (version 3.7.1) for February 2016 as an example of GHG inflow. For this simulation, initial and boundary conditions for the background concentration of CO_2 are provided by NOAA ESRL's CarbonTracker Near Real-Time (CT-NRT; https://www.esrl.noaa.gov/gmd/ccgg/carbontracker/CT-NRT/), which has a resolution of 1 degree and 3 hourly output and anthropogenic emissions are provided by the Vulcan 2.2 emissions with hourly data at 0.1 degree from 2012, and biogenic fluxes are provided hourly by coupling WRF meteorology to the Vegetation Global Atmosphere Soil model (VEGAS; Zeng et al., [2005]).

Figure 8 demonstrates that vertical mixing and advection-diffusion modifies mixing ratios as the PBL changes and air moves across the urban domain before it is sampled at a background tower throughout the month of February. The average particle travel time across the NEC-B/W is four to six hours. Assuming the background tower inlets are lower than the height of the mixed layer, modeled background mole fractions, in general, will be more enhanced than their associated observations at NEC-B/W towers made during well-mixed conditions later in the day. However, this is not always the case. The presented work illustrates this challenge. All the estimated background tower scaling factors, $\widehat{\boldsymbol{\beta}}$, from the geostatistical regression analysis in Section 4.1 are less than one for both February and July, indicating that enhancements need to be dampened to match the variability in their corresponding NEC-B/W observational mole fractions. In a real data application, these scaling factors would be unknown and thus, it would be difficult to determine the impact of atmospheric dynamics on a NEC-B/W GHG observation.

To overcome the impact of a diurnally changing mixed layer, some studies use observed mixing ratios from upwind background towers at the same time as those observed at urban towers sites for their modeled background values [e.g. Lauvaux et al., 2016; Turnbull et al., 2015]. These approaches assume that errors associated with changing meteorology and heterogenous fluxes have less impact than those from diurnally varying PBL dynamics. However, Figure 8 shows that the structure of the mixing ratios along the western wall of the NEC-B/W can change daily throughout the month. In addition, given the size of the NEC-B/W, structured incoming plumes may diffuse horizontally (Lauvaux, personal communication) by the time they reach an urban tower site. Thus, the incoming CO_2 mole fraction distribution is different vertically and horizontally during the average particle travel time across the NEC-B/W. The relative importance of errors from assuming temporal or spatial consistency when associating an observed mole fraction from an urban tower to an upstream observation using a Lagrangian framework remains unclear. To account for both errors, a more sophisticated approach may be required to appropriately isolate the background signal in the mixing ratios

observed at NEC-B/W towers locations such as combining in-situ observations with GHG modeled output.

Note that locating background towers using the method presented here is based on how well the observed mole fractions at the background towers explain the variability of the incoming CO_2, not explaining its overall magnitude. The method, and thus the selection of towers for the NEC-B/W, should not be impacted if the background enhancement is constantly biased high or low.

Finally, although atmospheric transport and dispersion modeling errors are not included in the synthetic observations for this study, we do not expect that adding Gaussian noise, as is typically done [e.g. Lopez-Coto et al., 2017; Lauvaux et al., 2016] to account for these errors in synthetic studies, will impact the selection of background tower locations. The addition of Gaussian noise would largely reduce the significance of estimated scaling factors, $\widehat{\boldsymbol{\beta}}$, associated with the selected background tower time series. More importantly, the true nature of atmospheric transport and dispersion modelling error is likely spatially and temporally correlated at urban scales. However, how to best represent this error structure in the model data mismatch matrix, **R**, has been largely unexplored; improperly representing these errors would bias the selection of background sites and thus, these errors are not included in this study. Nevertheless, the RMSDs and mean errors provided in this work provide a baseline for background error that can be used to compare against transport errors for urban domains in future work. It is assumed that transport errors are the dominate model data mismatch error as represented in **R** but background errors in urban areas, especially those like the NEC-B/W, could be of similar magnitude.

6 Concluding Remarks

This work presents the first application of statistical methods (i.e. combination of Bayesian Information Criteria and geostatistical regression) to help locate background towers for estimating urban GHG emissions using an inversion framework. The statistical methods are based on how well synthetic observations modeled at background towers explain the CO_2 variability in the incoming air. The methods identify four towers located around the edge of the NEC-B/W domain whose modeled background, in general, explains the "true" modeled background at the urban tower sites. However, the ability of the background tower synthetic observations to represent of the "true" modeled background is challenged in July, when the meteorology and extra-urban biogenic fluxes drive the variability of the total modeled enhancements at the NEC-B/W urban sites.

One of the limitations of this study is that the results are dependent on whether the flux variability in Vulcan v2.2 and CarbonTracker 2013b modeled output is reflective of the true variability in the underlying flux field. In addition, the results are also reliant on the performance of WRF-STILT. Applying the approach presented here to a larger ensemble of flux and

atmospheric-dispersion models, would be a way to explore this limitation, but it is unclear whether such work would yield different conclusions.

In addition, even though the large regional CH_4 sources are mostly collocated with those of CO_2 (SI Figure 1), the towers selected in this analysis may not be the optimal sites for explaining CH_4 enhancements as observed at the NEC-B/W towers due to some regional CH_4 emission differences. However, unlike CO_2 in the summer months, the background towers would not need to account for the large diurnal and seasonal variability in extra-urban biogenic CH_4 fluxes for the NEC-B/W.

Beyond demonstrating the method, the work presented illustrates that the use of multiple background towers provides a benefit in explaining the variability of CO_2 mole fraction in the incoming air masses on observations made in an urban domain. This is a critical limitation for estimating urban GHG emissions using top-down inversion methods with real observations in metropolitan areas, such as the NEC-B/W, downwind of significant fluxes and varied meteorology. The work also shows that, for such areas, background towers alone will not be sufficient to accurately isolate the background signals from the mixing ratios observed in the urban domain. Clearly, more sophisticated approaches, e.g. those that include the combination of in-situ measurements with modeled output, such as models that predict four dimensional GHG concentrations at the urban domain edges, must be considered to overcome errors in GHG emission estimates due to background conditions. This analysis suggests that these four-dimensional predicted concentrations should be generated using fluxes up to 550 km away and possibly farther for eastern urban domains such as the NEC-B/W. GHG observations from aircraft campaigns in the area could also be useful for characterizing the spatial gradients of background air along the edges of the city. Nevertheless, background towers will continue to be critical because they provide continuous observational constraints for representing incoming air mole fraction. A better representation of the background air mass will help reduce one of the more significant errors associated with urban GHG emission estimates using inversion approaches, which currently limits our understanding of city emissions.

Acknowledgments, Samples, and Data

We would like to thank the anonymous reviewers whose helpful comments significantly improved the quality of this manuscript. We also thank fellow researchers at NIST, specifically Subhomoy Ghosh, Kuldeep Prasad, and Tamae Wong and scientists at the University of Michigan including Eric Kort and Martín Hoecker-Martinez for providing input to this work. We acknowledge Anna Michalak at the Carnegie Institute for Science at Stanford University and Riley Duren at the Jet Propulsion Laboratory for providing computing resources for the STILT runs as well as data storage. The NIST reviews from Antonio Possolo and Eric Shirley also helped improve the manuscript. Finally, we would like to thank the following scientist and institutions for sharing their flux data: Kevin Gurney (Vulcan 2.2 fossil fuel emissions, University of Arizona State University) and the National Oceanic and Atmospheric Administration (NOAA CarbonTracker 2013b biospheric fluxes). Work by V. Yadav was

partially funded by an interagency agreement between NASA and NIST (IAA-2014-0020-0). Also, C. Martin contribution was funded under the NIST University of Maryland award 70NANB14H333.

The data used within this study is publicly available as cited in the manuscript text. Certain commercial equipment, instruments, or materials are identified in this paper in order to specify the experimental procedure adequately. Such identification is not intended to imply recommendation or endorsement by the National Institute of Standards and Technology, nor is it intended to imply that the materials or equipment identified are necessarily the best available for the purpose.

References

Breón, F. M., G. Broquet, V. Puygrenier, F. Chevallier, I. Xueref-Remy, M. Ramonet, E. Dieudonné, M. Lopez, M. Schmidt, O. Perrussel, and P. Ciais, (2015) An attempt at estimating Paris area CO_2 emissions from atmospheric concentration measurements, Atmos. Chem. Phys., 15, 1707-1724, doi:10.5194/acp-15-1707-2015

Cambaliza, M.O., P.B. Shepson, D. Caulton, B. Stirm, D. Samarov, K. Gurney, J. Turnbull, K.J. Davis, A. Possolo, A. Karion, C. Sweeney, B. Moser, A. Hendricks, T. Lauvaux, K. Mays, J. Whetstone, J. Huang, I. Razlivanov, N. Miles, and S.J. Richardson, (2014), Assessment of uncertainties of an aircraft-based mass-balance approach for quantifying urban greenhouse gas emissions. Atmos. Chem. Phys., 14, 9029-9050, www.atmos-chem-phys.net/14/9029/2014/ doi:10.5194/acp-14-9029-2014, 2014.

Davis, K.J., A. Deng, T. Lauvaux, N.L. Miles, S.J. Richardson, D.P. Sarmiento, K.R. Gurney, R.M. Hardesty, T.A. Bonin, W.A. Brewer, B.K. Lamb, P.B. Shepson, R.M. Harvey, M.O. Cambaliza, C. Sweeney, J.C. Turnbull, J. Whetstone and A. Karion, (2017) The Indianapolis Flux Experiment (INFLUX): A test-bed for developing urban greenhouse gas emission measurements. Elem Sci Anth, 5:21, DOI: http://doi.org/10.1525/elementa.188.

Duren, R.M and C.E. Miller (2012), Measuring the Carbon Emissions of Megacities, Nature Climate Change *2*, 560–562, doi:10.1038/nclimate1629

Fang, Y., Michalak, A. M., Shiga, Y. P., and Yadav, V. (2014) Using atmospheric observations to evaluate the spatiotemporal variability of CO_2 fluxes simulated by terrestrial biospheric models, Biogeosciences, 11, 6985-6997, doi:10.5194/bg-11-6985-2014

Gerbig C., J. C. Lin, S. C. Wofsy, B. C. Daube, A. E. Andrews, B. B. Stephens, P.S. Bakwin, and C. A. Grainger, (2003b) Toward constraining regional-scale fluxes of CO2 with atmospheric observations over a continent: 2. Analysis of COBRA data using a receptor-oriented framework, J. Geosphys. Res., 108(D24), 4757, doi:10.1029/2003JD003770

Gerbig, C., A. J. Dolman, and M. Heimann, (2009), On observational and modelling strategies targeted at regional carbon exchange over continents, Biogeosciences, 6(10), 1949-1959, doi:10.5194/bg-6-1949-2009

Gourdji, S.M., K.L. Mueller, V. Yadav**,** D.N. Huntzinger, A.E. Andrews, M. Trudeau, G. Petron, T. Nehrkorn, J. Eluszkiewicz, J. Henderson, D. Wen, J. Lin, M. Fischer, C. Sweeney, A.M. Michalak, (2012) North American CO_2 exchange: Inter-comparison of modeled estimates with results from a fine-scale atmospheric inversion, Biogeosciences, 9(1), 457-475, doi:10.5194/bg-9-457-2012.

Gurney, K.R., D. L. Mendoza, Y. Zhou, M. L. Fischer, C. C. Miller, S. Geethakumar, and S. de la Rue du Can (2009), High Resolution Fossil Fuel Combustion CO2 Emission Fluxes for the United States, Environmental Science & Technology, 43(14), 5535-5541, doi: 10.1021/es900806c

Huntzinger, D.N., S.M. Gourdji, K.L. Mueller, A.M. Michalak (2011) The utility of continuous atmospheric measurements for identifying biospheric CO_2 Flux Variability, J. Geosphys. Res. Atmos., 116 (D6), D06110, doi:10.1029/2010JD015048

Lauvaux, T., N.L. Miles, A. Deng, S.J. Richardson, M.O. Cambaliza, K.J. Davis, B. Gaudet, K.R. Gurney, J. Huang, D. O'Keeffe, Y. Song, A. Karion, T. Oda, R. Patarasuk, D. Sarmiento, P. Shepson, C. Sweeney, J. Turnbull, and K. Wu (2016) High resolution atmospheric inversion of urban CO2 emissions during the dormant season of the Indianapolis Flux Experiment (INFLUX), J. Geophys. Res., 121, doi:10.1002/2015JD024473

Lin, J. C., C. Gerbig, S. C. Wofsy, A. E. Andrews, B. C. Daube, K. J. Davis, and C. A. Grainger, (2003): A near-field tool for simulating the upstream influence of atmospheric observations: The Stochastic Time-Inverted Lagrangian Transport (STILT) model. J. Geophys. Res., 108, 4493, doi:10.1029/2002JD003161

Lopez-Coto, I., S. Ghosh, K. Prasad, J. Whetstone, (2017) Tower-Based Greenhouse Gas Measurement Network Design – the NIST North East Corridor Testbed, Advances in Atmospheric Sciences, doi 10.1007/s00376-017-6094-6

McKain, K., A. Down, S. M. Raciti, J. Budney, L. R. Hutyra, C. Floerchinger, S. C. Herndon, T. Nehrkorn, M. S. Zahniser, R. B. Jackson, N. Phillips, and S. C. Wofsy, (2015), Methane emissions from natural gas infrastructure and use in the urban region of Boston, Massachusetts, PNAS 2015 112 (7) 1941-1946; published ahead of print January 23, 2015, doi:10.1073/pnas.1416261112

Mueller, K.L., V. Yadav, P.S. Curtis, C. Vogel, and A.M. Michalak, (2010) Attributing the variability of eddy-covariance CO_2 flux measurements across temporal scales using geostatistical regression for a mixed northern hardwood forest, Global Biogeochemical Cycles, 24 (3), GB3023, doi:10.1029/2009GB003642

Peters W., A. R. Jacobson, C. Sweeney, A. E. Andrews, T. J. Conway, K. Masarie, J. B. Miller, L. M. P. Bruhwiler, Gabrielle Pétron, A. I. Hirsch, D. E. J. Worthy, G. R. van der Werf, J. T. Randerson, P. O. Wennberg, M. C. Krol, and P. P. Tans, (2007) An atmospheric perspective on North American carbon dioxide exchange: CarbonTracker, 104(48), 18925–18930, doi:10.1073/pnas.0708986104

Rayner, P.J., M.R. Raupach, M. Paget, M. P. Peylin, E. Koffi, (2010), A new global gridded data set of CO2 emissions from fossil fuel combustion: Methodology and evaluation, J. Geosphys. Res. Atmos., 115 (D19), 2156-2202, doi:10.1029/2009JD013439

Stein, A. F., R. R. Draxler, G. D. Rolph, B. J. B. Stunder, M.D. Cohen, and F. Ngan, (2015) 2015. NOAA's HYSPLIT atmospheric transport and dispersion modelling system, Bull. Am. Meteorol. Soc., 96, 2059–2077, doi:10.1175/BAMS-D-14-00110.1

Turnbull, J.C., C. Sweeney, A. Karion, T. Newberger, S.J. Lehmann, P. P. Tans, K. J. Davis, T. Lauvaux, N. L. Miles, S. J. Richardson, M. O. Cambiliza, P. B. Shepson, K. Gurney, R. Patarasuk, and I. Razlivanov, (2015) Toward quantification and source sector identification of fossil fuel CO_2 emissions from an urban area: Results from the INFLUX experiment, J. Geosphys. Res. Atmos., 120, doi:1002/2014JD022555

Verhulst, K., A. Karion, J. Kim, P. K. Salameh, C. Sloop, T. Pongetti, R. F. Keeling, S. Newman, V. Yadav, Clare Wong, F. M. Hopkins, P. Rao, J. Miller, R. F. Weiss, R. Duren, and C. Miller, (2016) Carbon Dioxide and Methane Measurements from the Los Angeles Megacity Carbon Project: 1. Calibration, Urban Enhancements, and Uncertainty Estimates, Atmos. Chem. And Phys. Discuss., doi:10.5194/acp-2016-850

Whelpdale, D. M., T. B. Low, and R. J. Kolomeychuk (1984), Advection climatology for the east coast of North America, Atmospheric Environment, 18(7), 1311-1327

Yadav, V., K.L. Mueller, D. Dragoni, A.M. Michalak (2010) A geostatistical synthesis study of factors affecting gross primary productivity in various ecosystems of North America, *Biogeosciences*, 7 (9), 2655-2671, doi:10.5194/bg-7-2655-2010

Yadav, V., K.L. Mueller, A.M. Michalak (2013) A backward elimination discrete optimization algorithm for model selection in spatio-temporal regression models, Environmental Modelling & Software, 42, 88-98, doi:10.1016/j.envsoft.2012.12.009

Zhang X., K. R. Gurney, P. Rayner, Y. Liu, and S. Asefi-Najafabady, (2014) Sensitivity of simulated CO_2 concentration to regridding of global fossil fuel CO_2 emissions, Geosci. Model Dev., 7, 2867–2874, doi: doi:10.5194/gmd-7-2867-2014

Zeng, N., A. Mariotti, and P. Wetzel, 2005: Terrestrial mechanisms of interannual CO_2 variability, Global Biogeochemical Cycles, 19, GB1016, doi:10.1029/2004GB002273

Location	Background Tower	February										July																
		Group 1					Group 2					Combined					Group 1					Group 2					Combined				
		1	2	3	4	5	1	2	3	4	5	1	2	3	4	5	1	2	3	4	5	1	2	3	4	5	1	2	3	4	5
North	9	x				x	x	**	*			x	x		x												x				
	8	x			x			x				**			x	**		x	x			x	x				*	*	x	*	*
	12	x	x	x			x											x		x	x	x	x			x					
South	5	*								**		x	x							x				x	x		**		**		**
	6													x	x																
	10			**		x		x									x					x					x			*	
	13																				**										
	14						x		x									*	*												
	15		x								x																				
Southwest	3			x							x	x					x							x		x					
	7				x	x				x						x			x		x		x		x			*	*	**	**
West	1		*		*		x			x			*	*	*	*			x					x	x	x		x			
	11			x					x		x			x			x			x	x					x		*			
Northwest	2				x	*		*	*	x	**		**	x		x	x	x					**							x	x
	4		x																	x		x		x	x				**		

Table 1: Results of both the BIC algorithm and the geostatistical approach. Groups 1 and 2 refer to the groups of NEC-B/W towers as identified in Figure 4. Only the five top models as selected by the BIC algorithms are shown for the sake of brevity. For each model, an 'x' indicates the background tower that was selected by the BIC. These five model combinations, comprised of different background tower mole fractions, are indicated under each category. The combined group represents all towers in the NEC-B/W urban area. The background towers noted with a (*, dark orange) are those background towers whose scaling factors are statistically significant to the 95% confidence level in its respective model. Those background towers noted with a (**, light orange) are those background towers with associated scaling factors that are statistically significant to the 66% confidence level.

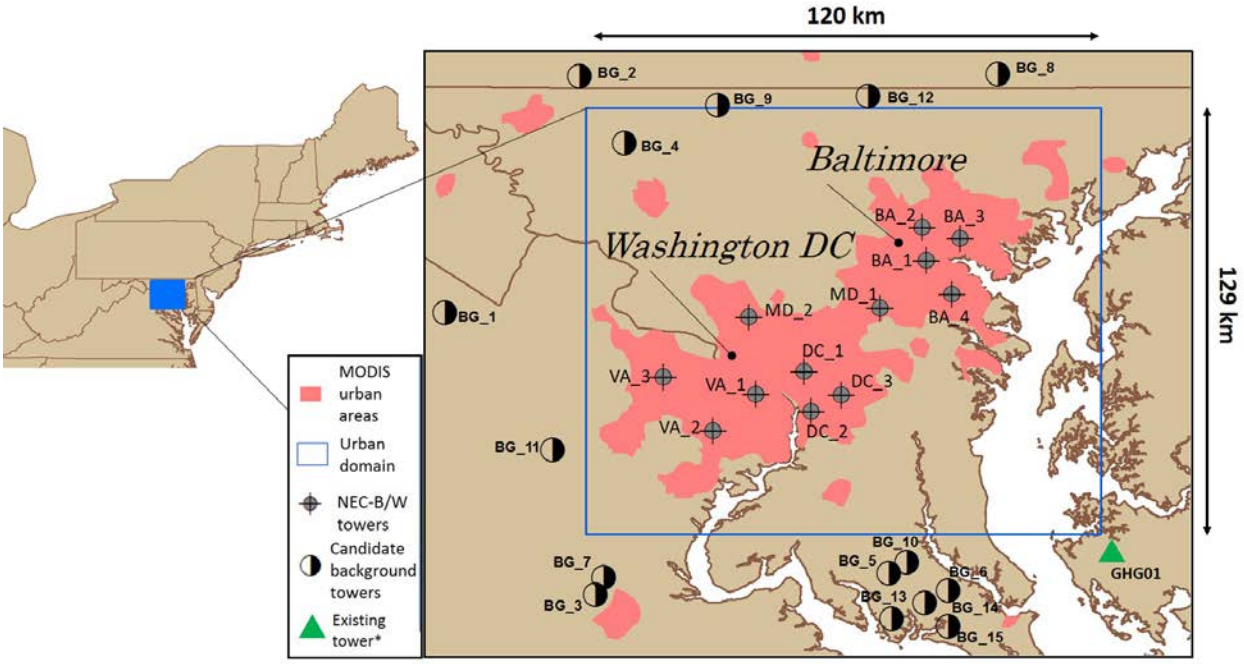

Figure 1: Site map for the Northeast Corridor (NEC-B/W) testbed. The blue box (NEC-B/W domain) is the area where GHG emissions fluxes will be estimated at a 1 – 2 km^2 resolution using atmospheric in-domain CO_2 observations from 12 urban tower locations shown (gray circles). Candidate background tower locations (black and white circles) are based on FCC towers filtered on specific conditions including height (~100m) and proximity to major emission sources. GHG01 (green triangle) is an existing in-situ tower location. At the time of this analysis, it was unclear whether this tower location would be available as a candidate tower location and thus, was not considered in the analysis (refer to Section 5). The red areas are urban extent as defined by MODIS 2012 (https://lpdaac.usgs.gov/dataset_discovery/modis/modis_products_table/mcd12q1). A table of both the NEC-B/W towers and potential background tower locations with their latitudes, longitudes, and height above ground level (AGL) is provided in Table S1.

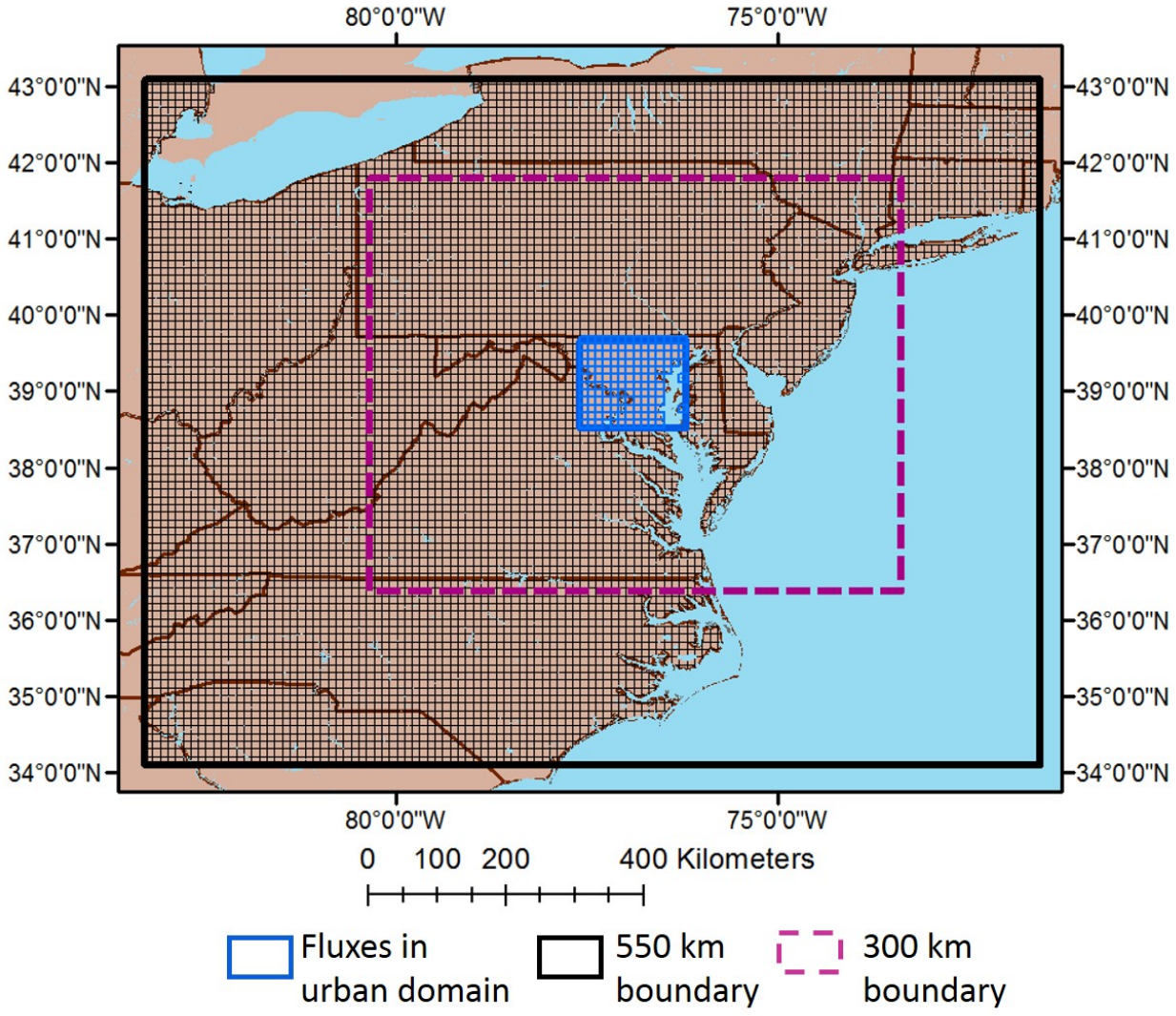

Figure 2: Representation of the two main areas for this study, i.e. the urban and extra-urban domains. $\boldsymbol{y}_{fossil\_ex}$ and $\boldsymbol{y}_{bio\_ex}$ are the CO_2 enhancements that enter the NEC-B/W urban domain due to sources and sinks (located in small black boxes) between the outer domain (thick black rectangle) and the NEC-B/W urban area (blue rectangle), and $\boldsymbol{y}_{fossil\_urb}$ and $\boldsymbol{y}_{bio\_urb}$ are mole-fraction enhancements at the NEC-B/W towers from sources and sinks in the NEC-B/W urban domain (blue box). The work presented also examines the influence of intermediate-field (300 km from the blue box, between blue and thick dashed magenta rectangle) and far-field (300 km

to 550 km which is the area between the thick magenta dashed and thick black rectangle) fluxes on CO_2 enhancements observed at the NEC-B/W tower sites (Section 3.2).

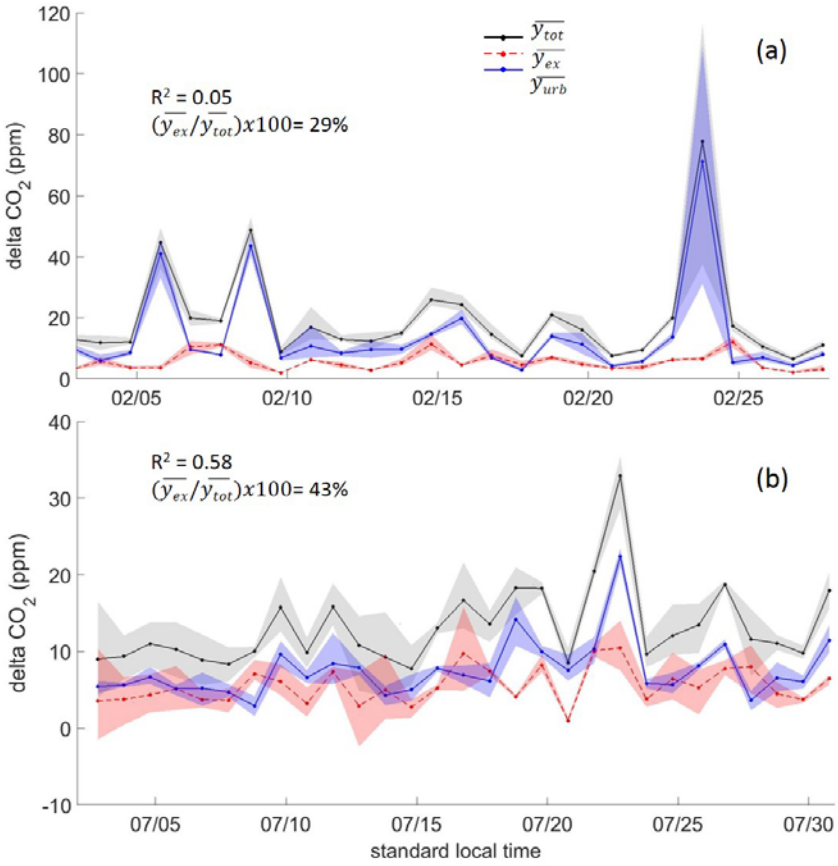

month	metric	VA_1	BA_4	DC_1	DC_3	DC_2	VA_2	VA_3	MD_1	MD_2	BA_1	BA_2	BA_3
Feb	$(\bar{y}_{ex}/\bar{y}_{tot})*100$	24%	35%	29%	36%	34%	31%	34%	30%	25%	21%	25%	30%
	R^2	0.04	0.05	0.04	0.10	0.07	0.03	0.12	0.02	0.08	0	0.01	0.02
Jul	$(\bar{y}_{ex}/\bar{y}_{tot})*100$	37%	45%	42%	49%	47%	45%	56%	41%	46%	31%	38%	39%
	R^2	0.69	0.71	0.67	0.63	0.62	0.77	0.87	0.62	0.62	0.70	0.63	0.55

Figure 3: Total modeled CO_2 mole-fraction enhancements ($\boldsymbol{y}_{tot}, ppm$) of (black line and points) of the daily mean of afternoon observations (12pm to 5pm local time) averaged across all the NEC-B/W towers for the months of February (subplot a) and July (subplot b) for 2013. Plots also include modeled CO_2 mole-fraction (ppm) from sources and sinks inside the NEC-B/W domain ($\boldsymbol{y}_{urb}$, solid blue line and points) and those from extra-urban fluxes ($\boldsymbol{y}_{ex}$, red dashed line and points). The shading around $\boldsymbol{y}_{tot}$, $\boldsymbol{y}_{ex}$, and $\boldsymbol{y}_{urb}$ represent the maximum and minimum modeled enhancement for a given afternoon period. The average $\boldsymbol{y}_{tot}$, $\boldsymbol{y}_{ex}$, and $\boldsymbol{y}_{urb}$ are 18.8 ppm, 5.7 ppm, and 13.4 ppm for February. For July, the average $\boldsymbol{y}_{tot}$, $\boldsymbol{y}_{ex}$, and $\boldsymbol{y}_{urb}$ are 14.4 ppm, 5.6 ppm, and 8.7 ppm. The associated table below the figure represents the ratio of the total synthetic enhancements ($\boldsymbol{y}_{tot\_i}$) to those associated with incoming air observed at each

NEC-B/W tower location ($\boldsymbol{y}_{ex\_i}$) for each month along with R^2 values. Real observations for February 2017 from the established NEC-B/W towers are consistent with the synthetic observations shown above both in terms of overall magnitudes and the variability of the time series (SI Figure 2). Note that the study does not include measurement error, but similar urban networks have reported a 0.1 to 0.2 ppm measurement uncertainties associated with hourly mole-fraction observations [Verhulst et al., 2016].

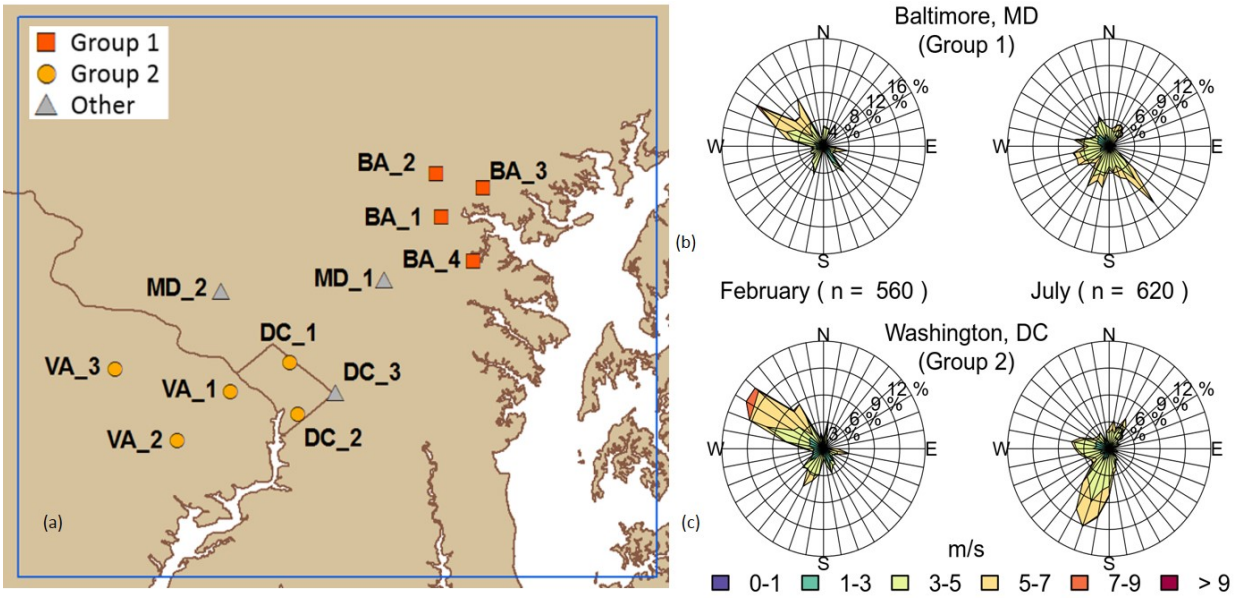

Figure 4: Location of the three groups of NEC/BW towers as identified by the correlation coefficients and root mean square differences of their CO_2 mole-fraction time-series representing sources and sinks from outside the urban domain (subplot a). Subplots (b & c) are the averaged wind roses associated with Group 1 (39.33ºN, 76.66ºW) and Group 2 (38.96ºW, 77ºN) towers generated from the WRF modeled output described in Section 2.1 for the months of February and July.

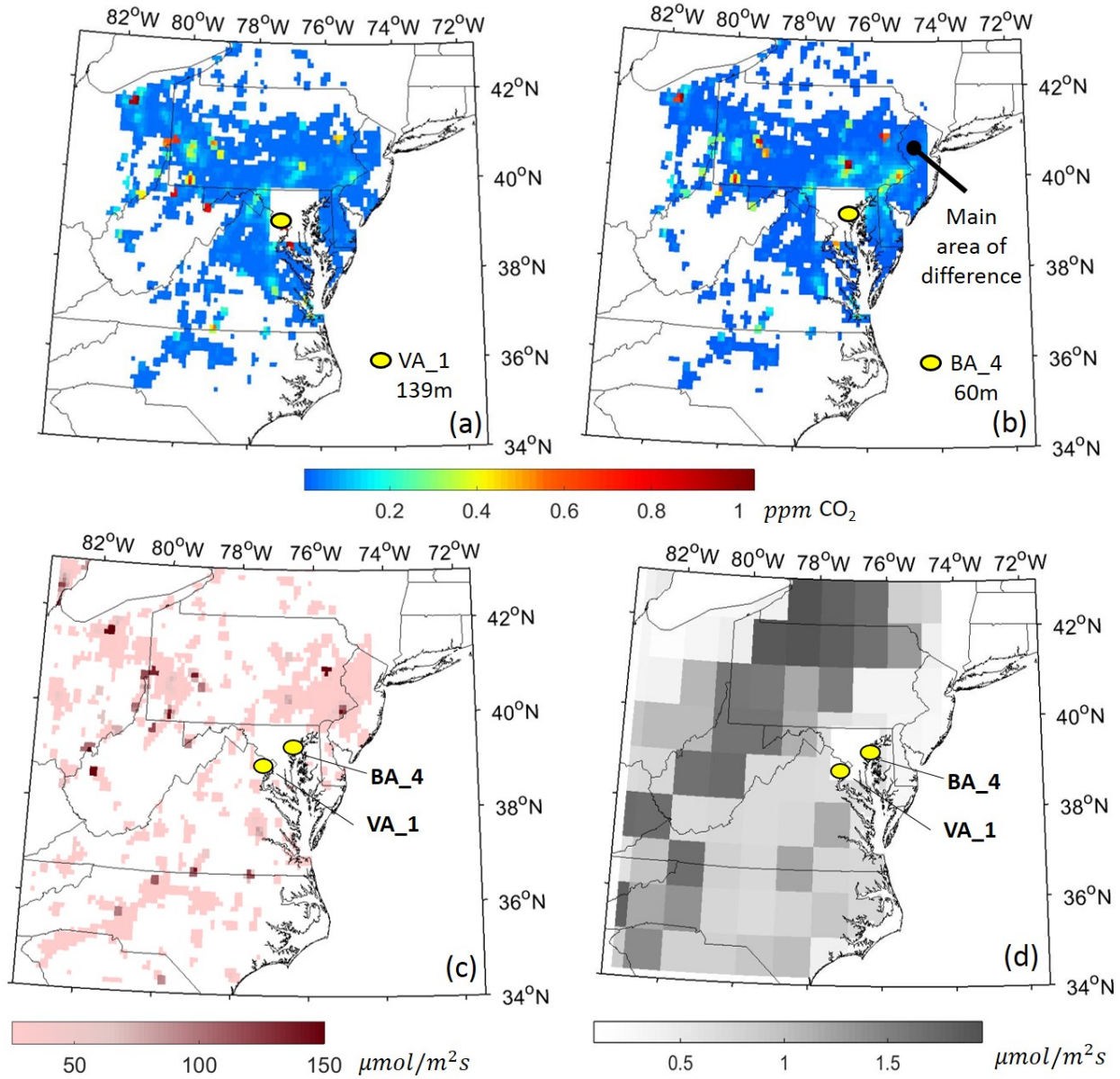

Figure 5: The average monthly contributions (ppm) from different source and sink locations outside the NEC-B/W urban domain to the hourly CO_2 mole-fractions as observed for February 2013 at NEC-B/W towers VA_1 (139m AGL – subplot a) and BA_4 (60m AGL – subplot b) whose sites are denoted by the yellow circle within the urban domain. White areas are areas that have less than a 0.015 ppm contribution to modeled enhancements at these two towers. Subplots

(c) and (d) are the monthly averaged Vulcan 2.2 emissions and CarbonTracker (CT) 2013b, respectively, used to create the synthetic observations for February. July contributions are provided in SI Figure 3.

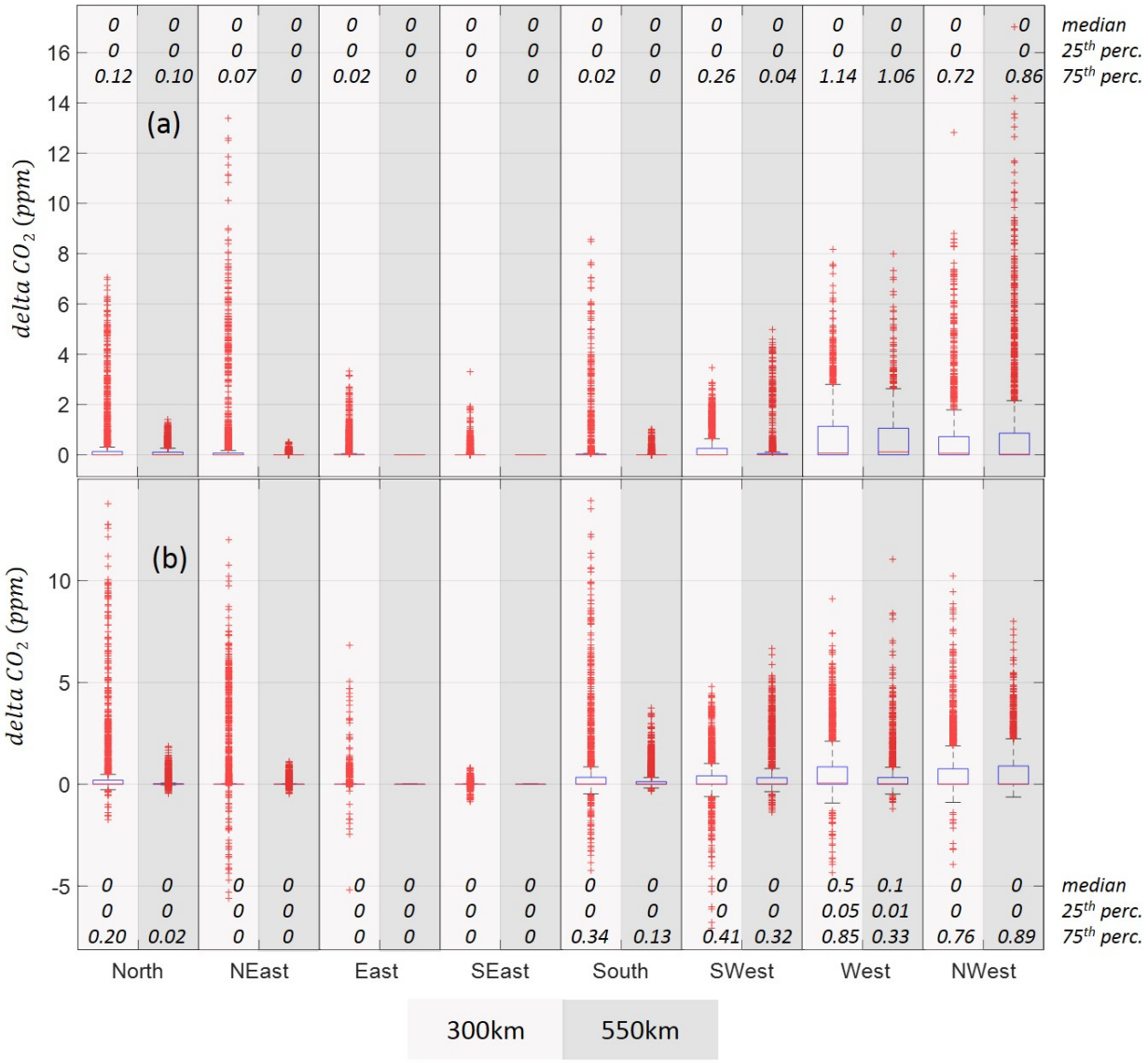

Figure 6: Boxplots of the simulated average contributions to all twelve NEC-B/W mole fractions ($\boldsymbol{y}_{ex}$) from extra-urban sources and sinks from different directions for February (subplot a) and July (subplot b), 2013. Far field contributions (300 km to 550 km) are in the dark gray rectangle boxes while the intermediate fields (urban domain to 300 km) are in the light grey rectangles. Red lines indicate the median with dashed bars indicating the 5th and 95th percentiles and outliers as red (+) symbols. The median, 25th, and 75th percentiles for February and July are also noted on each subplot. Note that although median values are small and

marginally similar, the extreme outliers have large impacts on the variability of the CO_2 enhancements as observed at the NEC-B/W tower sites.

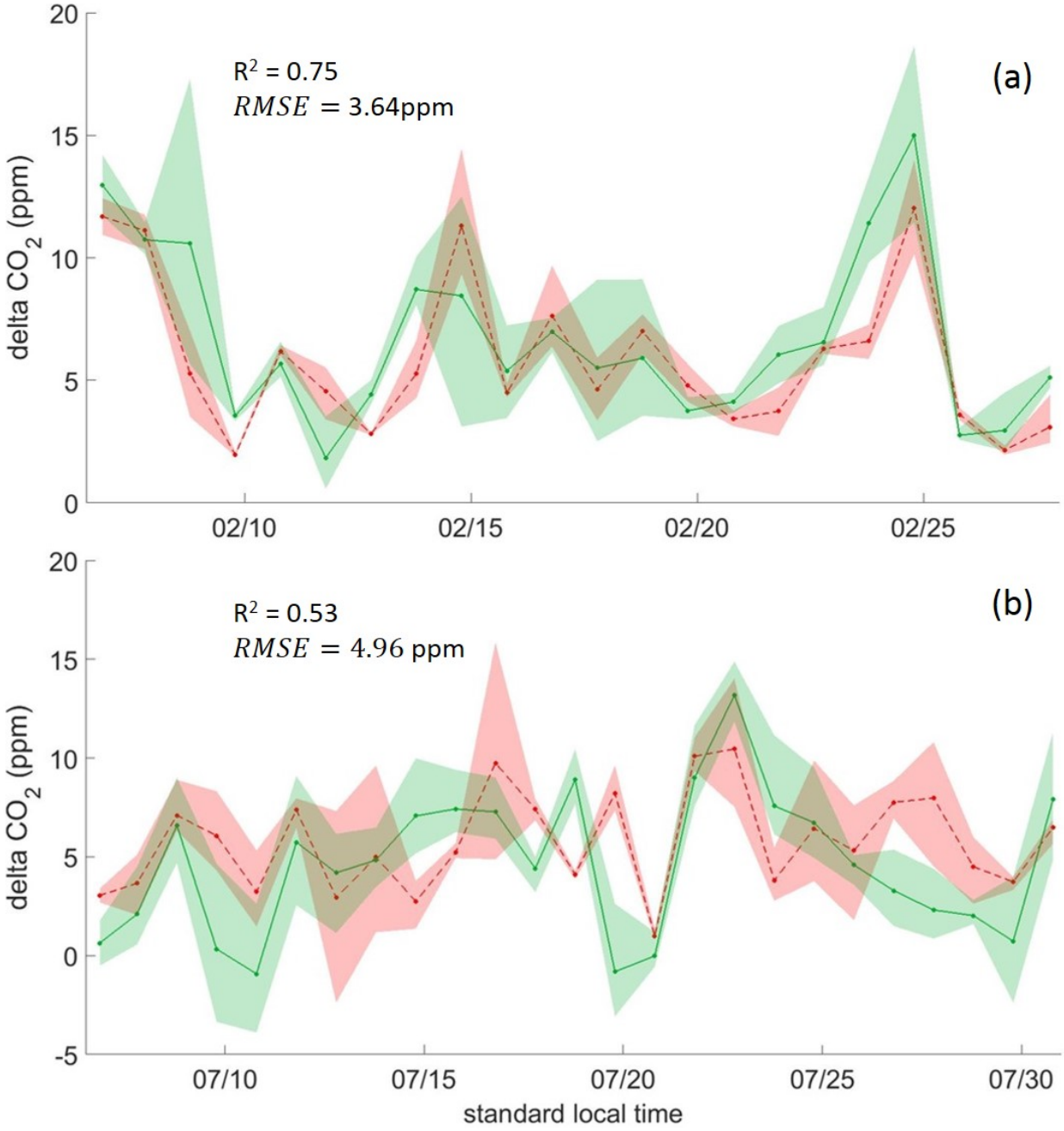

Figure 7: Estimated "background" time-series (modeled background using mole fractions from selected background towers, dashed red line with points) and $\boldsymbol{y}_{ex}$ (green line with points, aka

"truth") as averaged across the urban towers for February (subplot a) and July (subplot b). Daily mean averages of afternoon observations (12pm to 5pm local time) are shown. The shading around the red and green lines represent the maximum and minimum modeled enhancement for a given afternoon period. Note that although the modeled background generally captures the truth, there are large deviations at specific times in each month.

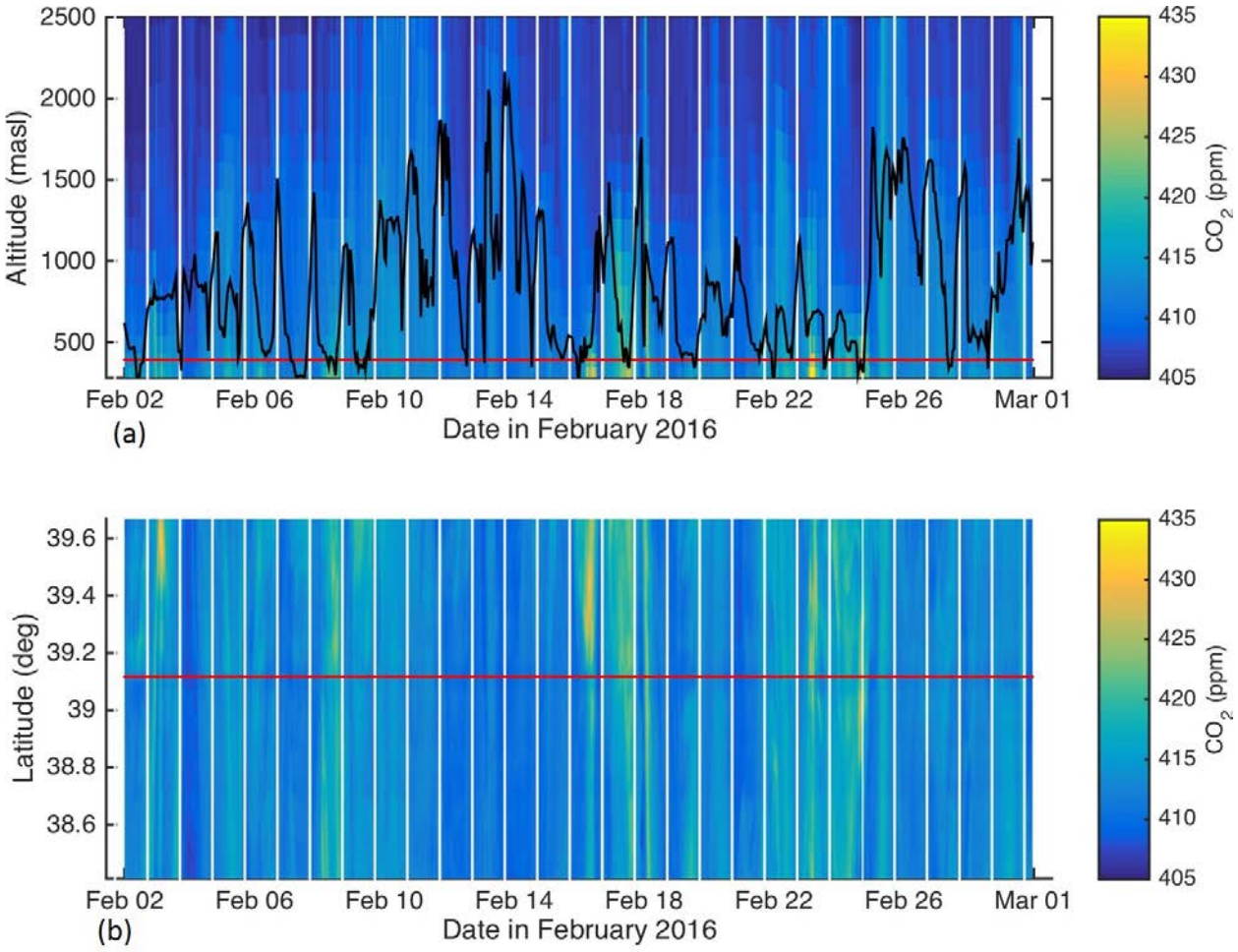

Figure 8: Subplot a are projected CO_2 mole fractions (ppm) for the location of BG_1. UTC (local time + 5h) time is represented on the x-axis and altitude (masl) on the y-axis. The color represents mole fractions in ppm throughout the vertical column and the white lines indicate local noon-time periods throughout the month. The black solid line is the PBL and the pink line is the inlet height at BG_1. Subplot b are projected CO_2 concentrations (ppm) along the western NEC-B/W boundary. The pink line indicates the latitude of the BG_1 along this wall. This

figure for February 2016 provides an example of the variability in time and space of incoming CO_2 that is representative of the winter period (February 2013) used in this study.